Sociedade Brasileira de Automática (SBA)
XV Simpósio Brasileiro de Automação Inteligente - SBAI 2021, 17 a 20 de outubro de 2021

Multivariable closed-loop control for layer geometry in Wire-Arc Additive Manufacturing ⋆

Rafael M. Bendia, Fernando Lizarralde and Fernando G. Coutinho

* *Programa de Eng. Elétrica, COPPE, Universidade Federal do Rio de Janeiro, Brasil*

Abstract: This paper focuses on modelling and control of mass and heat transfer process for Wire Arc Additive Manufacturing (WAAM). It considers a nonlinear model for the deposited layer geometry of thin walls bases on process variables (wire feed speed, arc current, travel speed and contact tip to workpiece distance) and physical variables (arc power, inter-pass temperature) as inputs. The model is based on the Rosenthal solution for the temperature distribution due to a moving heat source in combination with a layer geometry parameterization, which is incorporated in a dynamic model of the GMAW process for control design. A closed-loop control is proposed to guarantee a more accurate deposition geometry considering the linearized model about a given operating point. Numerical simulation results illustrate the efficacy of the proposed control for the regulation and tracking of both layer height and wall width and a experimental setup for validating the control strategy is also proposed.

Keywords: Additive manufacturing, process control, nonlinear control, optimal control,

1. INTRODUCTION

Wire Arc Additive Manufacturing (WAAM) is a large-scale metal Additive Manufacturing (AM) technology that uses an arc welding process to produce metal parts additively. It offers a viable alternative to traditional manufacturing, with a wide range of use cases in industries such as aerospace, marine, oil&gas and automotive (Almeida and Williams (2010), Martina et al. (2013)). WAAM works by melting metal wire using an electric arc as the heat source. The wire, when melted, is then deposited in the form of beads on the substrate. As the beads join together, they create a single layer of material. The process is then repeated, layer by layer, with bead position controlled by a robotic arm, until the metal part is completed. WAAM can work with a wide range of wire materials, such as stainless steel, nickel-based alloys, titanium alloys and aluminum alloys.

In order for WAAM to produce a near net-shape parts with no internal defects and with the desired material properties, a closed-loop control system is essential, as it is able to act during the process to keep key variables within their operational specifications, while rejecting process disturbances introduced by material impurities, wire deviation, fumes, among other causes.

Improving the accuracy of the layer geometry during deposition leads to decreased material consumption and post processing machining. Both, layer height and wall width, have a direct impact on the final geometry of the produced part. If the deposited bead width is smaller than expected, the part may not be completely filled by the material, beads that should overlap may not, leading to internal voids in the final part (Li et al., 2018). Otherwise, if the deposited bead is wider than planned, the final part will be larger than needed, requiring more machining to achieve the final form. Larger than planned beads also mean that a greater part of the beads are overlapped, creating a distortion on the height of the layer. The accumulated error on each layer can lead to a deformed final geometry and act as a disturbance to the planned Contact Tip to Workpiece Distance (CTWD), which takes a toll on the general quality of the deposition, causing spatter, possible transfer mode change and creating disturbances for the bead width as well.

This work proposes a control oriented physics-based model for the WAAM process layer geometry. The control problem (Figure 1) consists in regulating the layer height h and wall width w, which are the most relevant geometric variables in WAAM. The controlled variables are the wire feed speed f, the power source current I_r, the Contact Tip to Workpiece Distance (CTWD) l_c and the travel speed v.

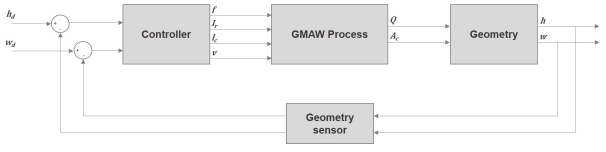

Fig. 1. WAAM layer geometry control scheme. h: layer height; w: wall width; f: wire feed speed; I_r: power source current; l_c: contact tip to workpiece distance; v: travel speed; A_c: cross-section area; Q: net power.

The process model considers two parts, a dynamic model of the Gas Metal Arc Welding (GMAW) process, including

⋆ This work was financed in part by Shell Brasil Petróleo Ltda, Embrapii and ANP, CNPq, the Coordenacao de Aperfeicoamento de Pessoal de Nivel Superior - Brasil (CAPES) - Finance Code 001.

mass and energy transfer equations, and a static model for the geometry. The GMAW process outputs are the net power into the material Q and the cross section area of the deposited layer A_c. Figure 2 highlights the differences between the cross-section area of a single bead and the cross-section area of a layer in WAAM. The geometry model establishes the relationship between the inputs, Q and A_c, and the outputs, h and w.

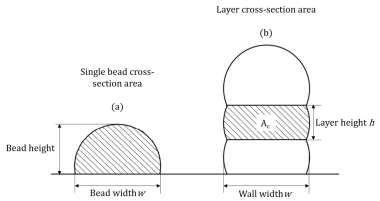

Fig. 2. (a) Cross-section area of a single pass bead and (b) Cross-section area of a layer in WAAM

Control of arc welding processes have a well established literature ((Suzuki et al., 1991),(Moore et al., 1998)). However regarding WAAM there are still few dedicated efforts (Xiong and Zhang, 2014). Although similar for using the same deposition processes, the concern with part geometry and material properties, as well as the interaction between layers present in WAAM makes that results for arc welding cannot be readily extended to WAAM. This paper proposes a closed loop control considering the linearized layer geometry model about a given operation point. A classical LQR is proposed for the h and w_e control while accounting for model uncertainties and measurement noise. Finally, an experimental setup is proposed to implement and validate the control.

2. LAYER GEOMETRY MODEL

A fifth-order nonlinear model of the GMAW process (Figure 3) considering the electrical dynamics of the power source and the dynamics of the forming molten metal droplet was introduced by Moore et al. (1997) and Naidu et al. (2003). This model describes the process behaviour in a globular-spray transfer mode. In Menezes et al. (2019) a similar model for a GMAW process working in the short-circuit transfer mode is proposed.

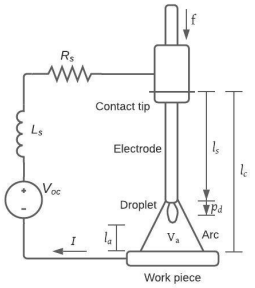

Fig. 3. Electrical model of the GMAW process

Here, the mass and energy transfer occurring during the deposition is modeled, regardless of the transfer mode, based on the input variables (deposition current I, wire feed speed f, CTWD l_c and travel speed v). The outputs of interest in this model are the power Q transferred to the material and the deposit cross section area A_c. Therefore, two modifications are made from the literature: 1) A control loop is introduced in the electrical circuit, in order to emulate a current-controlled power source, instead of voltage-controlled power source. 2) In order to model the mass transfer, the droplet dynamics is simplified by a volumetric balance assuming that the wire stickout is much larger than the melted electrode.

The energy transfer is modelled by the power source dynamics, which is given by:

$$\frac{dI}{dt} = \frac{1}{L_s}\left(V_{oc} - (R_a + R_s + R_L)\ I - V_0 - E_a(l_c - l_s)\right) \quad (1)$$

where L_s is the source inductance, V_{oc} is the source open-circuit voltage, R_s is the source resistance, R_a is the arc resistance, R_L is the electrode resistance, V_0 is the constant charge zone, E_a is the arc length factor and l_s is the wire stickout. The electrode resistance R_L depends on its length:

$$R_L = \rho\ [l_s + 0.5\ (r_d + p_d)] \quad (2)$$

where ρ is the resistivity of the electrode, r_d is the droplet radius and p_d is the distance between the droplet center of mass and the solid electrode. Assuming that $2l_s \gg r_d + p_d$ (i.e. the stickout is much larger than the melted electrode), R_L can be approximated by the stickout resistance $R_L = \rho\ l_s$, thus, the droplet dynamics can be neglected ((Moore et al., 1997) (Thomsen, 2004) (Anzehaee and Haeri, 2011)).

In order to consider a current-controlled power source where the deposition current I is driven to a reference current I_r, V_{oc} is used as a control variable defined by:

$$V_{oc} = K_v\ (I_r - I) + \bar{V}_{oc} \quad (3)$$

where $\bar{V}_{oc}$ is the open-circuit voltage operating point and K_v is a proportional gain. Therefore, the closed-loop current dynamic equation (1)–(3) is given by:

$$\frac{dI}{dt} = \frac{1}{L_s}\left[K_v I_r - (R_a + R_s + \rho l_s + K_v)I + \right. \\ \left. + \bar{V}_{oc} - V_0 - E_a(l_c - l_s)\right] \quad (4)$$

Additionally, the electric arc variables, arc voltage V_a and arc power $P_a = V_a\ I$, are given by:

$$V_a = V_0 + R_a\ I + E_a\ (l_c - l_s) \quad (5)$$

$$P_a = R_a\ I^2 + (E_a\ (l_c - l_s) + V_0)\ I \quad (6)$$

Finally, the rate of energy transferred from the arc to the workpiece is modelled by the process efficiency η, then the net power into the workpiece Q is given by:

$$Q = \eta P_a \quad (7)$$

The mass transfer is modelled as the difference between the material entering the system, which is a function of wire feed speed f, and the material leaving the system, which is the molten material. Assuming there is no change in the electrode density ρ_w due to the phase change, the inflow material is given by the volumetric flow into the system ($A_w\ f$), where A_w is the cross section area of the wire. The outflow material is given by the volumetric flow out of the system, which is the melting rate M_r. This leads to the following stickout dynamics,

$$A_w \frac{dl_s}{dt} = A_w\ f - M_r \tag{8}$$

The melting rate M_r is defined by (Moore et al., 1997):

$$M_r = C_2\rho\ l_s\ I^2 + C_1\ I \tag{9}$$

where C_1 and C_2 are melting rate constants.

From the perspective of a coordinate system moving alongside the torch with speed v, as shown in Figure 4, the deposited bead volumetric flow is defined as $\frac{dV}{dt} = A_c v$. The volume deposited to form the bead is equal to the outflow from of material from the power source system, which, from equation (8), is equal to M_r. Therefore, since $\frac{dV}{dt} = M_r$, from (9), A_c is given by:

$$A_c = (C_2\rho\ l_s\ I^2 + C_1\ I)/v \tag{10}$$

Then, the nonlinear dynamic system is given by:

$$\frac{dl_s}{dt} = -\frac{1}{A_w}(C_2\rho\ l_s\ I^2 + C_1\ I) + f \tag{11}$$
$$\frac{dI}{dt} = \frac{1}{L_s}\left[K_v I_r - (R_a + R_s + \rho l_s + K_v)I + \Delta V_0 - E_a(l_c - l_s)\right]$$

where the state variables are the wire stickout, l_s (m), and the deposition current, I (A), the input variables are the wire feed speed, f (m/s), and the reference current, I_r (A) with $\Delta V_0 = V_{oc} - V_0$. The output variables are the net power into the workpiece, Q (W), and the cross section area of the deposit, A_c (m^2):

$$Q = \eta\ \left(R_a\ I^2 + (E_a\ (l_c - l_s) + V_0)\ I\right) \tag{12}$$
$$A_c = (C_2\rho\ l_s\ I^2 + C_1\ I)\ v \tag{13}$$

Various models have been developed for predicting layer geometry in AM (Almeida and Williams, 2010), (Martina et al., 2013), (Xiong and Zhang, 2014) (Cruz et al., 2015). Regarding analytical models, Pinkerton and Li (2004) model the geometry of the melt pool for a Direct Laser Deposition AM process and more recently, Rios et al. (2018) propose a model for layer height and wall width in TIG and Plasma deposition. Both works are derived from the well known work of Rosenthal on moving heat sources (Rosenthal, 1941).

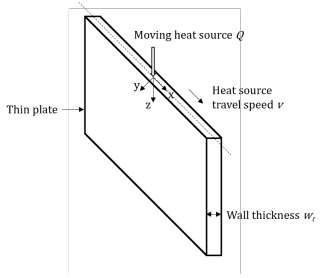

Fig. 4. Substrate in the Rosenthal solution for a thin wall.

In welding, the melt pool dimensions can be calculated from the temperature field in the substrate, around a moving point heat source. The isotherm curve corresponding to the melting temperature gives the shape of the melt pool. Rosenthal quasi-stationary solution to this heat transfer problem calculates the temperature field as a function of the power into the substrate and the travel speed of the heat source. Considering a thin wall substrate as shown in Figure 4, Rosenthal solution takes the following form:

$$T - T_0 = \frac{Q}{2\pi k w_t}\ K_0\left(\frac{r_{xz} v}{2\alpha}\right)\ e^{\left(-\frac{xv}{2\alpha}\right)} \tag{14}$$

where Q is the net power into the workpiece, T is the temperature at the (x, z) coordinate, x and z are the coordinates of a point relative to the position of the heat source, T_0 is the substrate temperature, k is the thermal conductivity, α is the thermal diffusivity, w_t is the wall thickness, v is the travel speed, $r_{xz} = \sqrt{x^2 + z^2}$ and K_0 is a zero-order modified Bessel function of the second kind.

In (Rios et al., 2018), an extension of the Rosenthal solution (14) for calculating the desired weld power in term of the well pool dimensions, is adapted for additive manufacturing by establishing the following relationship:

$$Q = 4kw_e\ (T_m - T_0)\ (0.2 + \frac{v}{2\alpha}d_a) \tag{15}$$

where T_m is the melting temperature, w_e is the effective wall width and d_a is the apparent weld pool depth (Fig. 5).

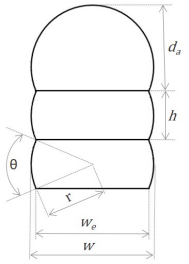

Fig. 5. Parameterization of the cross-section area of a layer

Here, we aim to rewrite equation (15) to provide a direct method to calculate the layer height h and the effective wall width w_e from the net power into the workpiece Q, the inter-pass temperature T_0, the travel speed v and the cross section area A_c of the deposited layer.

The cross section area of a deposited bead is assumed to be circular. This is valid if the radius $r < 6$mm (Rios et al., 2018). Figure 5 shows the layer geometry for a circular cross section area. The geometric features (w, w_e, h and d_a) are established as follows:

$$w = 2r\ ; \quad w_e = 2r\cos(\theta/2)\ ; \quad h = 2r\sin(\theta/2)\ ;$$
$$d_a = \frac{w + h}{2} \tag{16}$$

The relationship between w, w_e and h is given by the cross section area of a single layer A_c:

$$A_c = 0.5\ (w^2 atan(h/w_e) + w_e h) \tag{17}$$

Considering the useful area given by the product $w_e h$, then the deposition efficiency η_d is defined as the ratio between the useful area and the total area A_c:

$$\eta_d = w_e h / A_c \tag{18}$$

Another criterion for the validity of circular cross section area (Rios et al., 2018), states that $\eta_d > 0.9$, which translates to $h < w/2$. Thus, considering $h < \frac{w_e}{2} < \frac{w}{2}$, then $\frac{h}{w_e} < \frac{1}{2}$ and $atan(h/w_e) \approx h/w_e$, A_c can be expressed as:

$$A_c = \frac{1}{2}\left(w^2\frac{h}{w_e} + w_e h\right) \tag{19}$$

Substituting (19) in (18), the relationship between w and w_e is obtained:

$$w = \sqrt{(2-\eta_d)/\eta_d}\; w_e \tag{20}$$

Thus, considering (16) and (19) in (15), the effective wall width can be expressed as a function of the process parameters Q and v and of the deposit cross section area A_c. The resulting quadratic equation is given by:

$$\sqrt{(2-\eta_d)/\eta_d}\; w_e^2 + 0.8\frac{\alpha}{v}\; w_e + \eta_d A_c - \frac{Q\;\alpha}{k\Delta T\; v} = 0 \tag{21}$$

where $\Delta T = T_m - T_0$. The $2nd$ order polynomial in w_e (21) has real roots if the root product $p = \left(\eta_d A_c - \frac{Q\alpha}{k\Delta T\; v}\right) / \sqrt{\frac{2-\eta_d}{\eta_d}}$ is negative. Condition $p < 0$ is guaranteed, since $0 \leq \eta_d \leq 1$, if the following condition is satisfied:

$$Q > \frac{k\Delta T v}{\alpha}\eta_d A_c \tag{22}$$

The stationary solution for the volumetric balance makes it possible to calculate the steady state value of the cross section area $A_c = A_w f/v$. Therefore, Condition (22) can be rewritten in term of f, which is an input to the deposition process:

$$Q > \frac{\eta_d\; k\Delta T A_w}{\alpha}\; f \tag{23}$$

which makes it possible to determine if the layer geometry model is valid at steady state.

Thus if condition (23) is satisfied, w_e and h are given by:

$$w_e = -\frac{0.4\alpha}{k_w v} + \sqrt{\left(\frac{0.4\alpha}{k_w v}\right)^2 - \frac{1}{k_w}\left(\frac{2A_c}{k_w^2+1} - \frac{Q\alpha}{k\Delta T v}\right)} \tag{24}$$

$$h = \eta_d\; \frac{A_c}{w_e} \tag{25}$$

where $k_w = \sqrt{(2-\eta_d)/\eta_d}$.

2.1 Model linearization

The proposed nonlinear model is linearized about an operational point in order to assess local stability and to allow linear control design. The linearized model is given by:

$$\dot{x} = A\; x + B\; u \quad ; \qquad y = C\; x \tag{26}$$

where the deviation variables are:

$$x = \begin{bmatrix} x_1 \\ x_2 \end{bmatrix} = \begin{bmatrix} l_s - l_{so} \\ I - I_o \end{bmatrix}; \quad u = \begin{bmatrix} u_1 \\ u_2 \end{bmatrix} = \begin{bmatrix} f - f_o \\ I_r - I_{ro} \end{bmatrix};$$

$$y = \begin{bmatrix} y_1 \\ y_2 \end{bmatrix} = \begin{bmatrix} w_e - w_{eo} \\ h - h_o \end{bmatrix} \tag{27}$$

and

$$A = \begin{bmatrix} -C_2\rho I_o^2/A_w & -(C_1 + 2C_2\rho l_{so} I_o)/A_w \\ (E_a - \rho I_o)/L_s & -(R_a + R_s + \rho l_{so} + K_v)/L_s \end{bmatrix} \tag{28}$$

$$B = \begin{bmatrix} 1 & 0 \\ 0 & K_v/L_s \end{bmatrix} \tag{29}$$

$$C = \begin{bmatrix} \overset{c_{11}}{\overbrace{\dfrac{c_{21}}{w_{eo}} - \dfrac{c_{11}A_{co}}{w_{eo}^2}}} & \overset{c_{12}}{\overbrace{\dfrac{c_{22}}{w_{eo}} - \dfrac{c_{12}A_{co}}{w_{eo}^2}}} \end{bmatrix} \tag{30}$$

The partial derivatives at operational point are given by:

$$c_{11} = \frac{1}{2k_w v\sqrt{\Delta_o}}\left(\frac{-2C_2\rho I_o^2}{k_w^2+1} - \frac{\eta\alpha E_a I_o}{k\Delta T}\right) \tag{31}$$

$$c_{12} = \frac{1}{2k_w v\sqrt{\Delta_o}}\left(-2\;\frac{2C_2\rho l_{so} I_o + C_1}{k_w^2+1} + \frac{\eta\alpha\;\left(2R_a I_o + E_a(l_c - l_{so}) + V_o\right)}{k\Delta T}\right) \tag{32}$$

$$c_{21} = (\eta_d C_2 \rho I_o^2)/v; \quad c_{22} = \eta_d\left(C_1 + 2C_2\rho l_{so} I_o\right)/v \tag{33}$$

where

$$\Delta_o = \left(0.2\frac{2\alpha}{k_w\; v}\right)^2 - \frac{1}{k_w v}\left(\frac{2\left(C_2\rho l_{so} I_o^2 + C_1 I_o\right)}{k_w^2+1} - \frac{\eta\alpha\left(R_a I_o + E_a(l_c - l_{so}) + V_o\right) I_o}{k\Delta T}\right)$$

and

$$A_{co} = \eta_d\left(C_2\rho\; l_{so}\; I_o^2 + C_1\; I_o\right)/v \tag{34}$$

3. CONTROL DESIGN

Closed-loop control strategies for GMAW process can be found in (Naidu et al., 2003) (Cruz et al., 2015). However, WAAM process brings a very challenging problem where even a control-oriented model is a coupled multivariable nonlinear system. Only recently, closed-loop control for wire-arc additive manufacturing has capture the attention of the community (Xiong and Zhang, 2014), (Xiong et al., 2016) (Xiong et al., 2020b) (Xiong et al., 2020a) (Li et al., 2021). In (Bendia et al., 2021) the system identification and preliminaries results using a PI controller are presented for wall width and layer geometry control. Here, we extend this previous result to achieve disturbance rejection with minimum cost, an infinite-horizon Linear Quadratic Regulator. The choice of a LQR controller is justified by its proved performance, robustness and conceptual tune. In order to track changes to the outputs desired set-point r_1 and r_2, the system considers tracking errors $e_1 = r_1 - y_1$ and $e_2 = r_2 - y_2$. Furthermore, for robustness, an integral part is added considering the extended state given by $\bar{x} = [x_1\; x_2\; z_1\; z_2]^T$, where $\dot{z}_1 = e_1$ and $\dot{z}_2 = e_2$. The resulting extended system is given by:

$$\dot{x} = \bar{A}\;\bar{x} + \bar{B}\;u + E\;r \quad ; \quad y = \bar{C}\;\bar{x} \tag{35}$$

where $r = [r_1\; r_2]^T$ is the reference signal and,

$$\bar{A} = \begin{bmatrix} A & 0 \\ -C & 0 \end{bmatrix};\; \bar{B} = \begin{bmatrix} B \\ 0 \end{bmatrix};\; \bar{C} = [C\;0];\; E = \begin{bmatrix} 0 \\ I_2 \end{bmatrix} \tag{36}$$

with I_2 being the identity matrix of size 2.

The solution to the infinite-horizon LQR is a state feedback control $u = -K\bar{x}$ where the gain matrix K is obtained by solving the Riccati equation (Astrom and Murray, 2008):

$$\bar{A}^T P + P\bar{A} - P\bar{B}R^{-1}\bar{B}^T P + Q = 0 \tag{37}$$

and

$$K = R^{-1}\bar{B}^T P \tag{38}$$

4. SIMULATION RESULTS

The simulation of the proposed control considers that all states are measurables. Generally, the deposition current

(x_2) can be measured, but measuring wire stickout (x_1) is a challenging task, which could require the use of a state observer. The simulation considers the designed linear control to the nonlinear system and contemplates changes in r_1 and r_2, to verify reference tracking, and changes in l_c and T_0 to account for model uncertainties. To account for measurement disturbances, a different white noise signal with an order of magnitude of 10^{-5}m and a sampling time of 0.05 seconds is introduced in each of the systems outputs. The parameters used for simulation are (Bendia et al., 2021): $\eta = 0.655$, $\eta_d = 0.958$, $Ea = 723.2561$ V m^{-1}, $V_0 = 5.1792$ V, $R_a = 0.0201$ Ω, $R_s = 0.004$ Ω, $L_s = 0.14$ mH, $\bar{V}_{oc} = 31$ V, $K_v = 10$ Ω, $l_c = 0.010$ m, $v = 0.12$ m/s, $T_0 = 300$ K, $T_m = 1600$ K, $\rho = 0.1319$ Ω m^{-1}, $k = 24$ W m^{-1}K^{-1}, $\alpha = 7.79 \times 10^{-6}$ m^{2}s^{-1}, $C_1 = 3.2634 \times 10^{-10}$ m^3 A^{-1}s^{-1}, $C_2 = 1.1836 \times 10^{-9}$ m^3 W^{-1}s^{-1} and $r_w = 0.00060$ m denoting the radius of the cross section of the wire.

The operating point, $l_{so} = 0.0041\ m$, $I_o = 147.79\ A$, $f_o = 0.055\ m/s$, $I_{ro} = 146\ A$, $w_{eo} = 0.0041\ m$ and $h_o = 0.0012\ m$, was chosen from single bead experimental data as presented in (Bendia et al., 2021). The poles are $\lambda_1 = -3.047$ and $\lambda_2 = -7.161 \times 10^4$.

The choice of Q and R aims to scale the components of the LQR objective function while penalizing the tracking error. This is done by selecting diagonal matrices and incorporating a 10^6 factor to all the elements corresponding to the states and inputs with an order of magnitude of 10^{-3} (x_1, z_1, z_2 and u_1). After the scaling, the penalty to the tracking errors is selected to achieve a rise time of $0.5s$ without overshoot. No additional penalty is needed for the control actions, as they are smooth and within its range. Therefore, the selected Q and R matrices are:

$$Q = \text{diag}\{1 \times 10^6, 1, 10^6 \times 10^6, 10^6 \times 10^6\} \quad (39)$$

$$R = \text{diag}\{1 \times 10^6, 1\} \quad (40)$$

The resulting feedback gain K, from (37)-(38), is given by:

$$K = \begin{bmatrix} 15.19 & 7.70 \times 10^{-8} & 297.75 & -954.65 \\ -5.50 \times 10^3 & 0.41 & -9.55 \times 10^5 & -2.98 \times 10^5 \end{bmatrix}$$

Figure 6 shows the outputs response and control actions to changes in the reference values with different model uncertainties ($l_c = 15mm$ and $T_0 = 400K$). At $t = 2$s, the desired value (h_d) of h is changed to 2mm and at $t = 4$s, the desired value (w_{ed}) of w_e is changed to 3.5mm.

The proposed control was capable of tracking reference changes with no overshoot and was able to maintain performance in the presence of model uncertainties. The control actions were smooth and without oscillations, showing an improvement from the PI control tuning presented in (Bendia et al., 2021). The PI control achieved similar performance but with abrupt steps in the control actions, particularly I_r.

5. PROPOSED EXPERIMENTAL SETUP

In order to evaluate the proposed closed-loop control, a robotic deposition system is used. Details about the available hardware and the ROS-based framework for controlling both the robot and the power source are described. The proposed architecture allows online changes

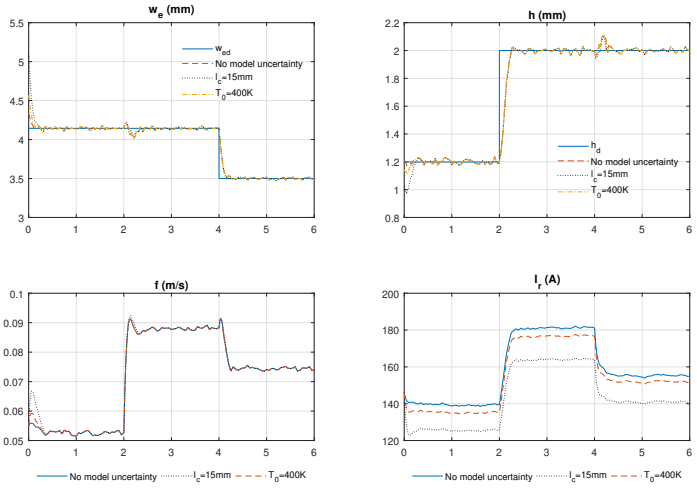

Fig. 6. Simulation results for different model uncertainties (l_c and T_0): setpoint changes at $t = 2$s, $h_d = 2$mm and at $t = 4$s, $w_{ed} = 3.5$mm at $t = 4$s.

in the power source deposition parameters and estimates the deposited bead width and height, enabling the closed loop control and its experimental validation.

The WAAM robotic set used by this experiment includes a 6-DoF Kuka KR90 and a 2-DoF Kuka positioning table, both connected to the same controller (KRC4). A Fronius Welding Power source is connected to the KRC4 through the Ethernet/IP protocol. The data exchanged by the Fronius power source and the KRC4 is set in an IO table, which includes the deposition commands and parameters. The robotic cell is presented in Figure 7a.

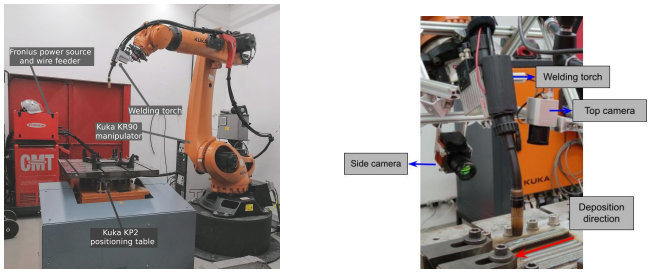

(a) (b)

Fig. 7. (a) Robotic cell. (b) Thermal cameras attached to the robot end-effector.

The KRC4 is equipped with the Kuka Robot Sensor Interface (RSI) software add-on installed, which allows interfacing the KRC4 with a PC over an ethernet connection using the User Datagram Protocol (UDP). The computer runs a modified version of the ROS *kuka_experimental* package to interface this connection with the KRC4.

The ROS *kuka_experimental* package provides tools to send joints position commands to the robot. The robot trajectory is planned as waypoints in the Cartesian space and a KDL (Kinematics and Dynamics Library) inverse kinematic solver maps these waypoints in the joint space. The KRC4 IOs table is modified to make the power source welding commands and parameters being sent by a RSI program. The ROS package is also adapted to exchange data with the power source indirectly, since all data

goes through the RSI program on the KRC4. A diagram illustrating this connection is presented in Figure 8.

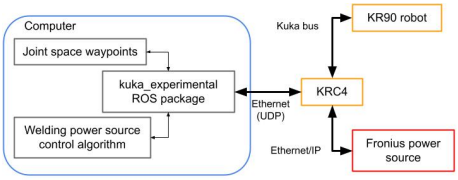

Fig. 8. Communication diagram between the personal computer and the robotic cell components.

In order to measure the bead's width and height for feedback control, a set of two thermal cameras is used. Several works are focused on real-time detection of the bead height and width using vision-based sensors (Xiong and Zhang (2013), Pinto-Lopera et al. (2016), Couto et al. (2020)). The proposed setup for the cameras is shown in Figure 7b.

For the proposed setup, a infrared camera with high-speed frame rates is positioned behind the torch, close to the deposition plan, giving a side view of the deposited bead to estimate the bead's height. This camera has adjustable range and is more suitable to the side view, pointing directly to the electric arc and being less affected by its light interference. Another thermal camera, with smaller frame rate but higher resolution is positioned beside the torch, giving a top view of the deposited bead so it can estimate its width. This camera has a range suitable to fit the glowing temperatures of the carbon steel (above 460º C). Figure 9 shows the side view camera image (on the left) and the top view camera image (on the right) from the specified setup during a deposition. The region of interest determines the area where the feature extracting algorithms are used to measure layer height.

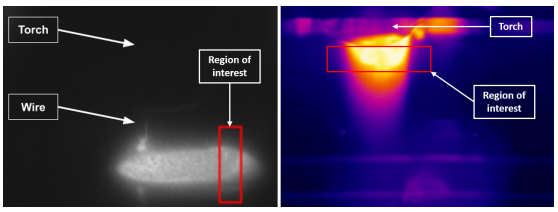

Fig. 9. Thermal images:(Left) Side view to measure layer height. (Right) Top view to measure weld pool width.

6. CONCLUSION

In this paper, a nonlinear state space model for layer geometry in WAAM is presented. It considers a dynamic model for the power source with a stationary solution for the heat transfer problem resulting in the layer geometry. The linearized model is used to design a LQR control to regulate and track setpoint changes for the wall width and layer height of a deposited part. The robotic system, a set of sensors and a ROS-based framework to implement the closed-loop control are also presented in this work. The command of robot and power source, along with the data acquisition from the thermal cameras are functional and tested in open-loop. Future work include experimental validation of LQR control and inclusion of thermal control (cooling rate and the inter-pass temperature) in order to guarantee desired material properties.

REFERENCES

Almeida, P.S. and Williams, S. (2010). Innovative process model of Ti-6Al-4V additive layer manufacturing using cold metal transfer. In 21^{st} *Int. Solid Freeform Fabrication Symp.*, 25–26.

Anzehaee, M.M. and Haeri, M. (2011). Multivariable adaptive control of the bead profile geometry in gas metal arc welding with thermal scanning. *Control Eng. Practice*, 19(12), 1408–1422.

Astrom, K. and Murray, R. (2008). *Feedback Systems: an Introduction for Scientists and Engineers*. Princeton University Press.

Bendia, R.M., Lizarralde, F., Passos, A.V., and Oliveira, V.H.P.M. (2021). Dynamic GMAW process model for layer geometry control in wire arc additive manufacturing. In 8^{th} *Int. Symp. on Advances in Computational Heat Transfer*. Rio de Janeiro (Brazil).

Couto, M.O., Costa, R.R., Leite, A.C., Lizarralde, F., Rodrigues, A.G., and Payão-Filho, J.C. (2020). Weld Bead Width Measurement in a GMAW WAAM System by using Passive Vision. In *Anais do* 23^{o} *Congresso Brasileiro de Automática*.

Cruz, J.G., Torres, E.M., and Absi Alfaro, S.C. (2015). A methodology for modeling and control of weld bead width in the GMAW process. *Journal of the Brazilian Society of Mechanical Sciences and Eng.*, 37(1), 1529–1541.

Li, Y., Li, X., Zhang, G., Horvath, I., and Han, Q. (2021). Interlauer closed-loop control of forming geometries for wire and arc additive manufacturing based on fuzzy-logic inference. *Journal of Manufacturing Processes*, 63, 35–47.

Li, Y., Sun, Y., Han, Q., Zhang, G., and Horváth, I. (2018). Enhanced beads overlapping model for wire and arc additive manufacturing of multi-layer multi-bead metallic parts. *Journal of Materials Processing Technology*, 252, 838–848.

Martina, F., Williams, S., and Colegrove, P. (2013). Design of an empirical process model and algorithm for the tungsten inert gas wire+arc additive manufacture of Ti-6Al-4V components. In 24^{th} *Int. Solid Freeform Fabrication Symp.*, 697–707.

Menezes, L., Silva, A., and Alfaro, S. (2019). Modeling and simulation of the metal transfer on GMAW-S process. *Journal of the Brazilian Society of Mechanical Sciences and Eng.*, 41(550).

Moore, K.L., Naidu, D.S., Yender, R., and Tyler, J. (1997). Gas metal arc welding control: part 1 - modeling and analysis. *Nonlinear Analysis, Theory, Methods & Applications*, 30(5), 3101–3111.

Moore, K.L., Yender, R., Tyler, J., and Naidu, D.S. (1998). Modeling, calibration, and control-theoretic analysis of the GMAW process. In *Proc. of the American Control Conf.*, 1747–1751.

Naidu, D.S., Ozcelik, S., and Moore, K.L. (2003). *Modeling, Sensing and Control of Gas Metal Arc Welding*. Elsevier Science.

Pinkerton, A.J. and Li, L. (2004). Modelling the geometry of a moving laser melt pool and deposition track via energy mass balances. *Journal of Physics D: Applied Physics*, 37(14), 1885–1896.

Pinto-Lopera, J.E., Motta, J.M., and Alfaro, S.C. (2016). Real-time measurement of width and height of weld beads in GMAW processes. *Sensors*, 16(9).

Rios, S., Colegrove, P., Martina, F., and Williams, S. (2018). Analytical process model for wire + arc additive manufacture. *Additive Manufacturing*, 21, 651–657.

Rosenthal, D. (1941). Mathematical theory of heat distribution during welding and cutting. *Welding Journal*, 20(5), 220–234.

Suzuki, A., Hardt, D.E., and Valavani, L. (1991). Application of adaptive control theory to on-line GTA weld geometry regulation. *ASME. J. Dyn. Sys., Meas., Control.*, 113(1), 93–103.

Thomsen, J.S. (2004). *Advanced Control Methods for Optimization of Arc Welding*. Ph.D. thesis, Aalborg University, Denmark.

Xiong, J., Yin, Z., and Zhang, W. (2016). Closed-loop control of variable layer width for thin-walled parts in wire and arc additive manufacturing. *Journal of Materials Processing Technology*, 233(4), 100–106.

Xiong, J. and Zhang, G. (2013). Online measurement of bead geometry in GMAW-based additive manufacturing using passive vision. *Measurement Science and Technology*, 24(11), 5103–5110.

Xiong, J. and Zhang, G. (2014). Adaptive control of deposited height in GMAW-based layer additive manufacturing. *Journal of Materials Processing Technology*, 214(4), 962–968.

Xiong, J., Zhang1, Y., and Pi, Y. (2020a). Control of deposition height in waam using visual inspection of previous and current layers. *Journal of Intelligent Manufacturing*.

Xiong, J., Zhu, B., Chen, H., and Zheng, S. (2020b). Peak elimination of cross structures in wire and arc additive manufacturing using closed-loop control. *Journal of Manufacturing Processes*, 58, 368–376.